Steerable Flipping Elastic Robot That Leverages Elastic Energy Through Both Bending and Twisting Deformation

Kisuke Nonoyama, Noriyasu Iwamoto, *Member, IEEE*, and Takuya Umedachi

***Abstract*—Harnessing elastic energy for power amplification in robotic locomotion, inspired by living organisms' mechanisms, enables robots to achieve dynamic and rapid movements even with actuators of limited instantaneous power output. Previous research in this domain has employed multiple elastic elements and independently controlled the release timing of stored energy to facilitate scalable locomotion. This study proposes a novel approach by developing a flipping biped robot that leverages a single elastic element (its body) by applying multiple deformation modes to predetermine locomotion direction. The proposed robot exhibits straight flipping locomotion with bending deformation of its elastic body. Furthermore, the robot alters its flipping direction with an 'additional twist,' enabling two-dimensional locomotion. Our proposed robot demonstrates diverse capabilities through experimental validation, including steering, vertical wall climbing, and seamless locomotion transition between surfaces at different angles. This work showcases the potential of elastic energy utilization for versatile and agile soft-robotic locomotion.**

***Index Terms*—Climbing robots, soft robot applications, soft robot materials and design.**

I. Introduction

PRE-controlled ultrafast movements, produced through the utilization of elastic energy, are exhibited by some living organisms [1], [2], [3], [4]. For example, mantis shrimps can land a powerful punch to cause cavitation by using the energy stored in the elastic elements of its arm exoskeleton [5]. Behind this powerful punching action, there is the activity tuning of the extensor and flexor muscles involved in the elastic elements, which kinetically alters the blow [6]. In addition, toads can eject their tongues quickly like a catapult by recovering the elastic energy stored by activating the depressor mandibulae muscles at the opening time. Furthermore, behind this behavior, correlations between coordinated motor activity and kinematic output are found, which indicates that toads plan their movements in advance [7]. The power amplification mechanism using elastic energy enables quick and powerful movements that exceed the capabilities of the muscles [8]. However, the time scale of the motion is considerably short to control, or the object in motion cannot be controlled during the motion owing to inertia. Therefore, as in the case of the organisms mentioned above, the intensity and direction of motion must be regulated during energy accumulation.

Fig. 1. Steerable flipping elastic robot. The total weight is 54 g. The weight near the end point of the body (motor + gripper) is 20 g.

Engineering systems inspired by the organisms have been developed. In particular, these systems utilize elastic energy as amplification mechanisms to achieve instantaneous high performance [9], [10], [11], [12], [13], [14], [15], [16], [17]. A typical example is the robot that utilizes snap-through stemming from bistability [9], [10], [11], [12], [13], [14]. Bistable structures have two energetically stable postures and can generate rapid deformation in transitioning between the two postures. Controlling the transition can endow robots (even those with less agile actuators e.g., SMA) with high-speed movements, such as jumping and catching.

Received 8 May 2024; accepted 7 September 2024. Date of publication 3 October 2024; date of current version 15 October 2024. This article was recommended for publication by Associate Editor Amy Kyungwon Han and Editor Yong-Lae Park upon evaluation of the reviewers' comments. This work was supported by KAKENHI Grant-in-Aid for Scientific Research (B) under Grant 21H01289. *(Corresponding author: Takuya Umedachi.)*

The authors are with the Faculty of Textile Science and Technology, Shinshu University, Ueda 386-8567, Japan (e-mail: nonokisuke0817@gmail.com; iwamoto@shinshu-u.ac.jp; umedachi@shinshu-u.ac.jp).

This letter has supplementary downloadable material available at https://doi.org/10.1109/LRA.2024.3474470, provided by the authors.

Digital Object Identifier 10.1109/LRA.2024.3474470

TABLE I
ENGINEERING SYSTEMS WITH ELASTIC ELEMENT(S)

Robots	Elastic element		Movement
	No.	Deformation mode	
7 g robot [16]	1	bending	jumping
Insect-sized Jumper [17]	1	bending (bucking)	jumping
Upside-down brachiation robot [18]	1	bending	flipping
Soft bodied jumper [9]	2	bending (bucking)	various jumping
Untethered crawler [10]	1+	bending (bucking)	crawling, steering
This study	**1**	**bending, twisting**	**flipping & steering**

Roboticists have been providing robots with 'multiple elastic elements' to control the movement by the power amplification mechanism [9], [10] (see Table I). These robots utilize one deformation mode: the action of each elastic element is limited to the extension and contraction of a spring or the transition between two postures of a bistable structure. Therefore, adding elastic elements to a robot and controlling the timing of its energy release is a method of extending motion diversity. The above-mentioned works propose robots to utilize multiple elastic elements, which can jump by changing their posture or steer the direction of propulsion.

This study proposes to pre-control the direction of motion using the power amplification mechanism based on elastic energy sourced from a *single* elastic element of the robot with *multiple deformation modes* (Fig. 1). The results of the prototype demonstrate that the direction of the locomotion can be successfully controlled by exploiting the multiple deformation modes. The design contributes to the lightweight and slimming design of the body because the robot does not need multiple elastic elements for control to generate such versatile behaviors. This design is advantageous for systems using power amplification mechanisms because the design reduces the inertial load required for the actuator and the energy dissipation owing to flow resistance (in air or fluid) because of its weight and volume. The flipping biped robot presented in this letter can steer during the locomotion through bending and twisting deformation, which is developed based on a flipping biped robot with elastic energy through only bending deformation [18].

II. THE PROPOSED METHOD

A. How to Bend and Twist Body

This study proposes a method of applying rotations to an elastic body, whose resting shape is arc, using two motors, which adds bending (Fig. 2(d)) and twisting deformation (Fig. 2(e)). The bending deformation, which is a prerequisite for the flip, is reproduced by rotating the entire arc-shaped body with the endpoints of the body constrained (see Fig. 2(a)–(d)). The body has zero elastic energy in the state (a), and the body reaches the state (d) by rotating both edges of the body (b-c), indicating that the body is deformed in a pure bend in (d). When the positional constraint of one endpoint is released in this state (i.e., no twisting), the body can flip around the other endpoint, which produces straight locomotion (i.e., no steering).

After transitioning to the bending state (Fig. 2(d)), the body will have a twisting deformation in addition to bending by providing additional rotation at one or both endpoints (Fig. 2(e)). Releasing the positional constraint on one endpoint in this state allows this body to flip in a different direction from the straight locomotion while eliminating the twisted state. We investigated how the body behaves during flipping with a prototype machine, depending on the direction and magnitude of the applied rotations.

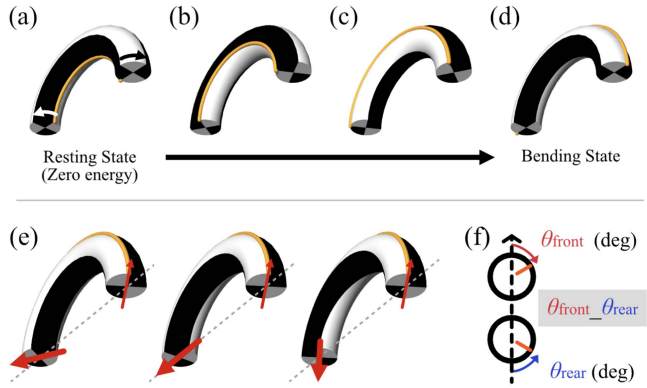

Fig. 2. Process of generating both bending and twisting deformations using rotational motion. The entire arc-shaped rod shown in black and white is an elastic body, and the orange line is a marking line to show that it has been rotated and twisted. (a)–(d) The process of transition from a state of no accumulated elastic energy to a state of pure bending. (e) Multiple deformation modes provided with bending and twisting. The illustration exemplifies how to provide additional rotation on one end (red emphasized arrows on the bottom). (f) Posture representation based on body rotation angle. The posture is represented by the rotation angles of the front and rear bodies, with the rotation angle in the bending state set to 0.

We define the notation of the body deformation posture owing to the complexity of the deformation modes (see Fig. 2(f)). The body deformation posture is expressed in the form "$\theta_{\mathrm{front}}\_\theta_{\mathrm{rear}}$." θ_{front} represents the rotation angle of the endpoint on the travel direction (front) side of the body; in the bending state (Fig. 2(d)), $\theta_{\mathrm{front}} = 0$. When the front endpoint is rotated 30 degrees clockwise from this state to apply a twisting deformation, $\theta_{\mathrm{front}} = 30$. Conversely, when the front endpoint is rotated 30 degrees anticlockwise, $\theta_{\mathrm{front}} = -30$. θ_{rear} also represents the opposite rotation angle of the endpoint on the rear; in the bending state, $\theta_{\mathrm{rear}} = 0$. From this state, θ_{rear} is 30 when the rear endpoint rotates 30 degrees anticlockwise, and $\theta_{\mathrm{rear}} = -30$ when the rear endpoint rotates 30 degrees clockwise.

B. Body Design

The body is made of arched corrugated beams, two of which are assembled in parallel (black upper part in Fig. 3). There are three reasons for this design: to allow for bending and twisting deformation of the body; to make it easy to manufacture with an FDM 3D printer; and to fully keep the motor inside the body to minimize interference when twisting the body (Fig. 3 lower part). The rubber band inside the arch contributes to the flipping motion as an elastic element. In a series of flipping motions, the body distortion is significant, and the body is highly affected by hysteresis. Therefore, we added the rubber band to the body for the prototype to utilize the energy accumulated in the band to

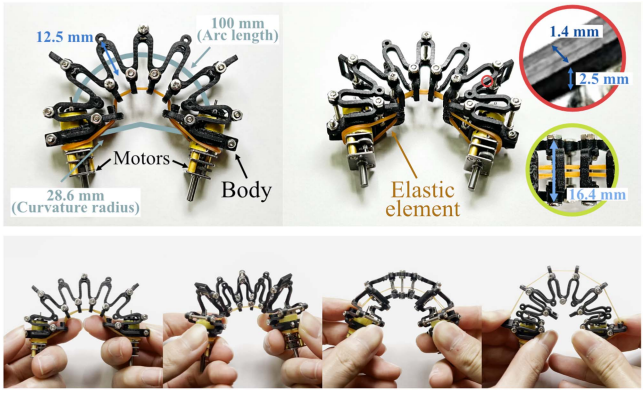

Fig. 3. Prototype body and its deformation process. Upper two photos: The body components and parameters. The body is shaped to allow bending and twisting. The rubber band inside the corrugated beams is an elastic element that contributes to the flipping motion. The motors at the endpoints of the body provide multiple deformation modes to the body through rotation. Lower snapshots: The process of performing bending deformation through rotation.

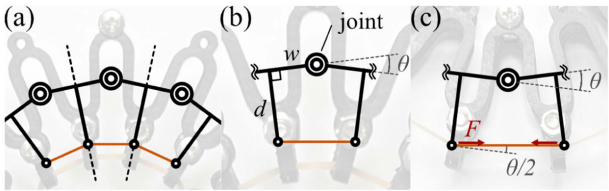

Fig. 4. Model of the body. The joint is equipped with a pseudo-torsion spring, the value of this spring is determined by the bending stiffness of the body and the tension of the rubber band.

perform the flipping motion. The body is made of Onyx, a nylon material containing carbon powder.

We determined the in-plane bending stiffness of this body from the bending stiffness of the corrugated beams and the tension of the rubber band. To achieve sufficient bending stiffness, we adjusted the tension of the rubber band by observing the flipping speed of the prototype. To determine the bending stiffness, we considered the body as the model shown in Fig. 4(a) and set the spring constant of the pseudo torsion spring (◎) installed at the joint of this one segment. The pseudo-spring constant k_{T} is determined as the sum of the spring constant k_{b} owing to the corrugated beams and the spring constant k_{r} due to the rubber band. k_{b} was obtained experimentally, and its value was 0.71 mN · m/deg. k_{r} is obtained from the displacement angle of the joint when the body is in the bending state (Fig. 2(d)) and the moment applied by the rubber band (Fig. 4(b) and (c)). When the displacement angle of the joint is 2θ and the moment applied to the joint by the rubber band is M, the relationship is $M = k_{\mathrm{r}} \cdot 2\theta$. Because M is expressed by the tension of the rubber band, k_{r} is governed by the following equation:

$$k_{\mathrm{r}} = \frac{F}{2\theta}\left(d\cos\frac{\theta}{2} - w\sin\frac{\theta}{2}\right). \tag{1}$$

In this prototype, $\theta = 25.7$ deg, $d = 9.60$ mm, $w = 7.12$ mm. Here, we set F to 4.44 N, resulting in $k_{\mathrm{r}} = 0.67$ mN · m/deg. Therefore, $k_{\mathrm{T}} = 1.38$ mN · m/deg. This prototype has seven of these single segments arranged in a row.

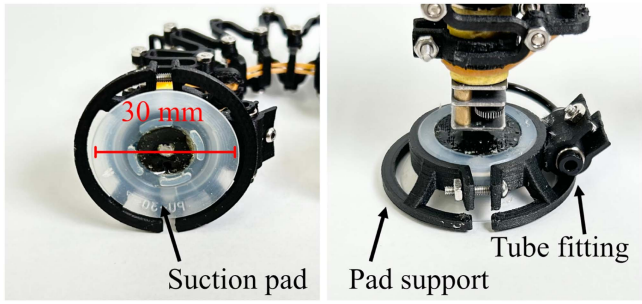

Fig. 5. Gripper of the prototype. The gripper consists of a suction pad to hold on the ground surface, a pad support part to prevent the suction pad deformation, and a tube fitting to connect the air tube. A neodymium magnet is inside the suction pad, which assists in flipping movement only on a vertical magnetic surface.

Motors attached to the ends of the body provide twisting deformation to the body through independent rotational motions. Because the flipping motion is produced by the elastic energy, independent of the motor speed, we can use motors with a high gear ratio. This prototype uses Pololu's Micro Metal Gearmotor with a gear ratio of 380:1.

C. Gripper Design

The gripper uses a suction pad, which can easily ensure gripping force to withstand flipping and switch gripping on and off (Fig. 5). To perform a flipping motion, the prototype requires a gripping force to stay on the ground surface. Our previous study of the upside-down brachiation robot [18] has shown that the gripper requires the maximum gripping force immediately 'after the start of flipping.' The force F_{flip} at this time on the newly proposed prototype was measured with a digital force gauge and found to be 4.6 N on average for ten times under the most severe conditions (the recoil of flipping and body weight are applied vertically to the suction pad.). Therefore, the diameter d of the suction pad is 30 mm according to the following equation.

$$d \geq 2\sqrt{\frac{F_{\mathrm{flip}}S}{\pi P}} = 2\sqrt{\frac{4.6 \cdot 8}{\pi \cdot 90000}} = 22.8(\mathrm{mm}) \tag{2}$$

where P is the vacuum pressure of the suction pad and S is the safety factor.

Gripping and releasing of the leg is realized with a solenoid valve (3 Port Solenoid Valve, S070B-5DC, SMC), where the output, supply, and exhaust ports are connected to the suction pad, vacuum pump (AC500XL, Makita), and nothing (the atmosphere) respectively. Gripping is achieved by connecting the suction pad with the vacuum pump to degas the inside of the suction pad. Gripping release is achieved by connecting the suction pad with the exhaust port to restore atmospheric pressure inside the suction pad.

The suction pad has a strong suction force perpendicular to the ground surface, but the suction force in the oblique direction becomes lower than the perpendicular grounding owing to the deformation of the pad. Therefore, a pad support/guide part (Fig. 5) is provided around the suction pads to prevent deformation owing to such oblique forces. The suction pad is

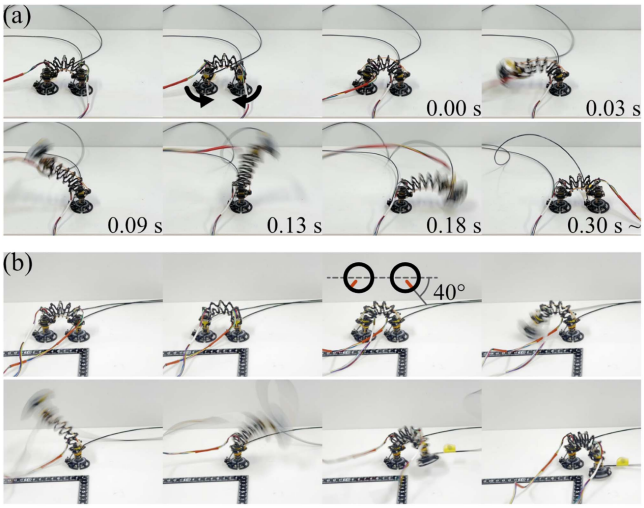

Fig. 6. Snapshots of the flipping motion of the prototype. (a) Flipping in 0_0 posture. The prototype flips without changing direction of travel by using only bending deformation. It takes 0.3 seconds for single flipping motion. (b) Flipping in 40_40 posture. The prototype changes direction of travel by flipping while eliminating twists.

equipped with a neodymium magnet[1] inside. The magnets were used to prevent the robot's swing legs from sagging away from the vertical wall owing to gravity during vertical locomotion. Sagging causes the suction pads to stop functioning (due to the distance from the wall), so the selection of the magnet was based on the dimensions of the ring shape that fits the suction pad rather than on the adsorption force of the magnet.

III. Results

A. Single Flip Through Bend and Twist Form

The prototype could successfully flip forward by releasing elastic energy via only bending deformation, as shown in Fig. 6(a). The consumed time in one step/flip (i.e., the time between the rear gripper releasing the ground and landing on the ground again) is 0.30 seconds. This motion requires an elastic energy charge (turning the body around the legs to deform the body), which requires a minimum time of 1.5 s. In total, at least 1.8 s is required per cycle. The robot travels 94 mm for one straight flipping. The maximum travel speed of the robot is approximately 63 mm/sec. The flipping posture is almost the same as the upside-down brachiation robot in the previous study [18].

Furthermore, the result also shows that the prototype acquired a steering function by releasing elastic energy via bending and twisting deformations, as can be observed in Fig. 6(b). The snapshots show the prototype flipping in the 40_40 posture. When the gripper released the ground, the prototype flipped while resolving its bending and twisting, landing the bouncing gripper in a different direction than the 0_0 posture.

[1]Misumi Parts No.: NOR273, N40, the suction force is 30 N (the vertical resistance force on a metal surface); however, when the pad is grounded, there is a 4–5 mm distance between the magnet and the ground, so the value is only for reference.), ring shape, diameter 21 x inner diameter 16 x thickness 2 (mm), NeoMag Co., Ltd.

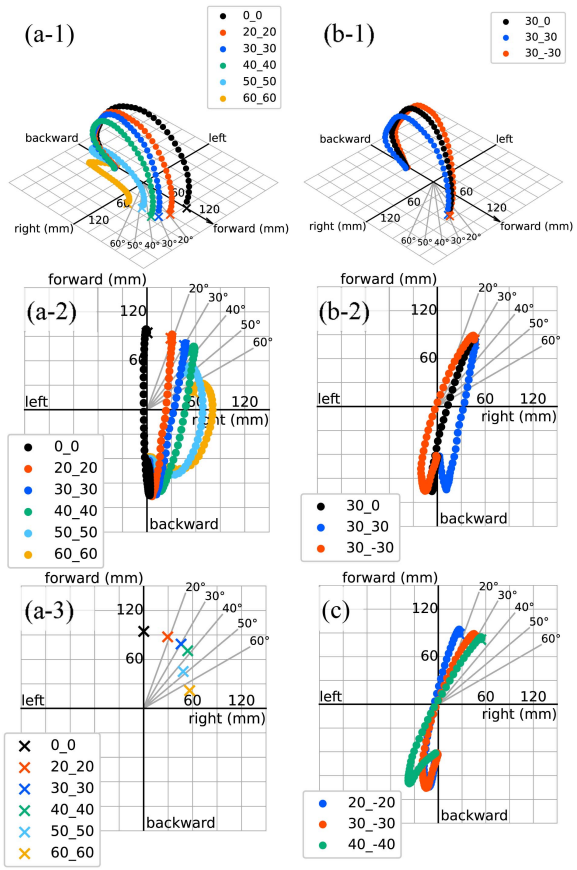

Fig. 7. Trajectories of the rear gripper when the prototype flips through various postures. The origin is the coordinates of the front gripper. (a) Flipping trajectories when $\theta_{\mathrm{front}} = \theta_{\mathrm{rear}}$. (a-1) is a bird's-eye view of the trajectory, (a-2) is a top view of the trajectory, and (a-3) is a top view of the landing points. The larger rotation angle is, the more significant the angular change in the direction of travel. However, no flipping was observed for $\theta_{\mathrm{front}} = \theta_{\mathrm{rear}} = 60$. (b) Difference in trajectories when the front body rotation angle remains fixed and the rear body rotation angle changes. (b-1) Is a bird's-eye view of the trajectory, and (b-2) is a top view of the trajectory. The rotational angle of the rear body hardly affects on the angular change in the direction of travel but is effects on the flipping trajectories. (c) Top view of flipping trajectories when $\theta_{\mathrm{front}} = -\theta_{\mathrm{rear}}$. The rear gripper passes directly above the front gripper.

B. Motion Captured Single Flip Through Variety Forms

We investigated how the flipping motion is steered when the prototype's body is twisted (i.e., by changing the body-twisting posture). Colored circles in Fig. 7 show the trajectory drawn by the rear gripper during flipping, with the front gripper as the origin, in 3D space for each body-twisting posture. The x marks in space are the coordinates of the rear gripper when it lands on the ground, projected onto the ground plane.

Fig. 7(a) shows the flipping trajectory of the prototype when $\theta_{\mathrm{front}} = \theta_{\mathrm{rear}}$. When θ_{front} and θ_{rear} range from 0 to 30 degrees, the body twist angle coincides with the steering angle. When θ_{front} and θ_{rear} are 40 degrees, the steering angle is less than the twist angle. However, the flipping operation was conducted without any problems. When θ_{front} and θ_{rear} are 50 degrees, the twisting strain on the body was high, the strain remained during the flipping motion, resulting in a crooked and distorted trajectory compared to the flipping trajectories when θ_{front} and θ_{rear} are up to 40 degrees. When θ_{front} and θ_{rear} are 60 degrees,

the flipping motion could not be performed (the swing leg did not go up and limped). The larger the value of θ_{front} and θ_{rear} up to 40 degrees, the greater the steering range, and the angular change in the direction of the prototype before and after flipping was consistent. Based on the above, it was decided to employ values up to 40 degrees for θ_{front} and θ_{rear} and conduct the following experiments.

Fig. 7(b-1) shows the difference in trajectories (bird's eye view) when θ_{front} remains fixed at 30 and $\theta_{\mathrm{rear}} = -30$, 0, and 30. The change in the twist angle of the rear body was ineffective on the angular change in the direction of the prototype before and after flipping. The landing position of the rear gripper did not change, but its trajectories were different. Fig. 7(b-2) shows the top view of (b-1), which demonstrates that the trajectory of the rear gripper passes directly above the front gripper at 30_-30 posture.

Moreover, we observed the trajectories when $\theta_{\mathrm{rear}} = -\theta_{\mathrm{front}}$, whose results are shown in Fig. 7(c). The trajectories in Fig. 7(b) and (c) are similar tendencies. When $\theta_{\mathrm{rear}} = -\theta_{\mathrm{front}}$, the steering angle is smaller than that with $\theta_{\mathrm{rear}} = \theta_{\mathrm{front}}$. Hence, postures with $\theta_{\mathrm{rear}} = -\theta_{\mathrm{front}}$ are not employed in the following experiments. When $\theta_{\mathrm{rear}} = 0$, the steering angle is the same as that when $\theta_{\mathrm{rear}} = \theta_{\mathrm{front}}$, but to provide symmetry bending and twisting deformation in the front and rear of the body, postures in $\theta_{\mathrm{rear}} = \theta_{\mathrm{front}}$ are employed in the following experiments.

The achieved motions are not 'completely' repeatable. The causes are assumed to be deformation accumulation of the elastic parts (creep and fatigue). It may be possible if the temperature of the elastic part is well controlled and we choose materials that do not (hardly) cause creep or fatigue.

C. Flipping Locomotion in Various Situations

Fig. 8 shows five locomotion sequences: (a) forward moving, (b) 90-degree steering, (c) obstacle bypassing, (d) vertical wall climbing, and (d) transition between planes. Based on the above-mentioned motion capture results, the prototype flips through $\theta_{\mathrm{front}} = \theta_{\mathrm{rear}}$ conditions ($-40 \leq \theta_{\mathrm{front}} = \theta_{\mathrm{rear}} \leq 40$) in this locomotion experiment. The robot was operated by a person who visually observed its status (suction, steering, and locomotion) and manually operated the front/rear motor angle and the suction pads' ON/OFF. Please note that the flipping locomotion experiments on the prototype were realized by utilizing multiple deformation modes.

Fig. 8(a) testifies that the prototype moved forward linearly by continuously flipping via the 0_0 posture. On the flat plane, the gripper holds ground firmly even when the prototype changed direction unintentionally, for example, owing to forces transmitted from the tethers. Even when such unintended direction changes occurred, the prototype could recover its direction of travel by steering through a twisting state. However, the prototype has four tethers (motor cables and air tubes) and a movement method that includes rotation; thus, the prototype's locomotion was limited by tether entanglement when excessive flipping was performed.

Fig. 8(b) and (c) show that the prototype moves while changing its direction of motion by flipping through the $\theta_{\mathrm{front}} = \theta_{\mathrm{rear}}$ state. In (b), the prototype flipped through 40_40, 40_40, and 20_20; consequently, it moved while changing direction by 90 degrees. In (c), the prototype flipped through 40_40, -40_-40, 40_40, and -40_-40; thus, it moved while bypassing obstacles.

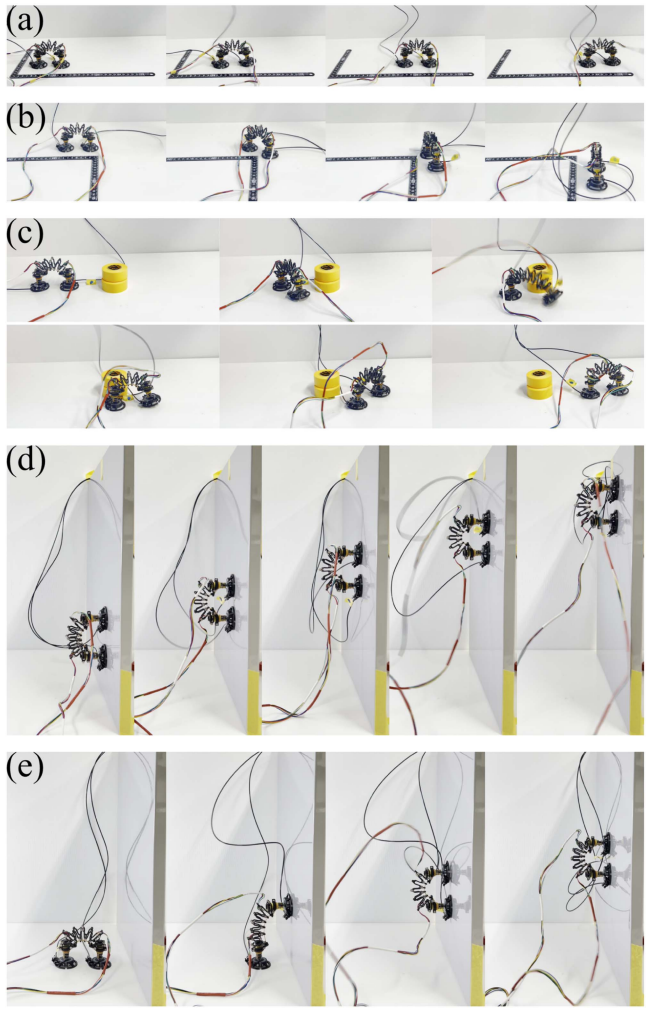

Fig. 8. Snapshots of locomotion performed by the fabricated prototype. (a) Forward moving, (b) 90-degree steering, (c) obstacle bypassing, (d) vertical wall climbing, and (e) transition between planes.

The snapshots in Fig. 8(d) and (e) demonstrate vertical wall climbing and transition between planes. The prototype successfully performed continuous flipping on a vertical wall surface and, can produce locomotion from a horizontal to a vertical plane. This movement is advantageous characteristic of the flipping biped robots, which can extend their two-dimensional planar movement into three dimensions. The success rate of the transition between planes depends on the distance between the front gripper and the plane before the transition, but this success rate could be increased by adjusting the position of the prototype using the steering function. Please note that this robot is not designed to increase energy efficiency but to increase the speed of the flipping process in locomotion. This is important for climbing robots, where the time spent supporting the body with only one leg can be reduced.

IV. Conclusion and Future Work

This letter demonstrates that providing multiple deformation modes to a single elastic element of a robot can increase its behavioral diversity and locomotion functionality (e.g., steering) on a worm-like elastic robot that utilizes a power amplification mechanism. Precisely, the flipping motion via only bending deformation can produce straight locomotion, whereas the flipping motion via bending as well as twisting deformation can change the direction of motion during the locomotion. The steering angle depends on the degree of twist of the body. The experiment demonstrates that the method enables the prototype to make a 90-degrees turn and bypass an obstacle. The prototype has demonstrated the ability to climb vertical walls and transition between planes with different angles. These results show a new possibility of controlling motion of soft-bodied robots using elastic energy.

Further research should be based on the development of the motion simulator of the flipping robot. Simulations are necessary to investigate the changes in flipping behavior owing to bending stiffness other than in the arch direction and twist (or torsional) stiffness of the body, which could not be discussed in this study, and to investigate the usefulness of flipping with large twisting angles (for example, when $\theta_{\mathrm{rear}} = -\theta_{\mathrm{front}}$). We did not prepare the simulations in this study because it would be costly to produce a 3D model to which bending and twisting could be applied. Even if we complete the simulator, the design constraints of a unique motion method for using a motor and body fabrication using an FDM 3D printer made it challenging to reflect the simulator's parameters in the body. The characteristics of a typical power amplification mechanism are determined by a combination of four elements: an elastic element to store energy, a latch to release energy, an actuator to provide energy, and the weight of the body that provides energy [19]. The preparation of simulations is indispensable in determining such a combination. If we can conduct a thorough simulation investigation, we should find a suitable body size and deformation mode for the flipping motion, as well as a body and grippers design consistent with these characteristics. Another direction of further research is untethering the robot. One possible method is to make the system pumpless. For this purpose, the flipping motion should be controlled more precisely so that the impact of the landing can be used for the adsorption motion.

References

[1] O. Vincent et al., "Ultra-fast underwater suction traps," *Proc. Roy. Soc. B: Biol. Sci.*, vol. 278, no. 1720, pp. 2909–2914, 2011.

[2] R. S. James and R. S. Wilson, "Explosive jumping: Extreme morphological and physiological specializations of Australian rocket frogs (litoria nasuta)," *Physiol. Biochem. Zool.*, vol. 81, no. 2, pp. 176–185, 2008.

[3] S. N. Patek, J. E. Baio, B. L. Fisher, and A. V. Suarez, "Multifunctionality and mechanical origins: Ballistic jaw propulsion in trap-jaw ants," *Proc. Nat. Acad. Sci.*, vol. 103, no. 34, pp. 12787–12792, 2006.

[4] S. M. Deban, J. C. O'Reilly, U. Dicke, and J. L. V. Leeuwen, "Extremely high-power tongue projection in plethodontid salamanders," *J. Exp. Biol.*, vol. 210, no. 4, pp. 655–667, 2007.

[5] S. N. Patek, W. L. Korff, and R. L. Caldwell, "Deadly strike mechanism of a mantis shrimp," *Nature*, vol. 428, no. 6985, pp. 819–820, 2004.

[6] K. Kagaya and S. N. Patek, "Feed-forward motor control of ultrafast, ballistic movements," *J. Exp. Biol.*, vol. 219, no. 3, pp. 319–333, 2016.

[7] A. K. Lappin, J. A. Monroy, J. Q. Pilarski, E. D. Zepnewski, D. J. Pierotti, and K. C. Nishikawa, "Storage and recovery of elastic potential energy powers ballistic prey capture in toads," *J. Exp. Biol.*, vol. 209, no. 13, pp. 2535–2553, 2006.

[8] T. J. Roberts and E. Azizi, "Flexible mechanisms: The diverse roles of biological springs in vertebrate movement," *J. Exp. Biol.*, vol. 214, no. 3, pp. 353–361, 2011.

[9] S. Nishikawa, Y. Arai, R. Niiyama, and Y. Kuniyoshi, "Coordinated use of structure-integrated bistable actuation modules for agile locomotion," *IEEE Robot. Automat. Lett.*, vol. 3, no. 2, pp. 1018–1024, Apr. 2018.

[10] T. Chen, O. R. Bilal, K. Shea, and C. Daraio, "Harnessing bistability for directional propulsion of soft, untethered robots," *Proc. Nat. Acad. Sci.*, vol. 115, no. 22, pp. 5698–5702, 2018.

[11] J.-S. Koh et al., "Jumping on water: Surface tension–dominated jumping of water striders and robotic insects," *Science*, vol. 349, no. 6247, pp. 517–521, 2015.

[12] S. W. Kim, J. S. Koh, J. G. Lee, J. Ryu, M. Cho, and K. J. Cho, "Flytrap-inspired robot using structurally integrated actuation based on bistability and a developable surface," *Bioinspiration Biomimetics*, vol. 9, no. 3, 2014, Art. no. 036004.

[13] Y. Horioka, M. Shimizu, and T. Umedachi, "A crawling robot that utilizes propagation of deformation waves of a bistable lattice actuated by a single motor," in *Proc. 2023 IEEE Int. Conf. Soft Robot.*, 2023, pp. 1–7.

[14] K. Shimura, N. Iwamoto, and T. Umedachi, "Bistable tensegrity robot with jumping repeatability based on rigid plate-shaped compressors," in *Proc. 2023 IEEE/RSJ Int. Conf. Intell. Robots Syst.*, 2023, pp. 8324–8330.

[15] F. Ito, Y. Ishii, S. Kurumaya, K. Kagaya, and T. Nakamura, "Instantaneous force generation mechanism based on the striking motion of mantis shrimp—design and control method of cavitation by simulation and experiment," *IEEE Robot. Automat. Lett.*, vol. 7, no. 4, pp. 9342–9349, Oct. 2022.

[16] M. Kovac, M. Fuchs, A. Guignard, J.-C. Zufferey, and D. Floreano, "A miniature 7G jumping robot," in *Proc. 2008 IEEE Int. Conf. Robot. Automat.*, 2008, pp. 373–378.

[17] R. Kurniawan et al., "An untethered 216-mg insect-sized jumping robot with wireless power transmission," in *Proc. 2020 IEEE/RSJ Int. Conf. Intell. Robots Syst.*, 2020, pp. 7881–7886.

[18] K. Nonoyama, M. Shimizu, and T. Umedachi, "Upside-down brachiation robot using elastic energy stored through soft body deformation," *IEEE Robot. Automat. Lett.*, vol. 7, no. 4, pp. 11291–11297, Oct. 2022.

[19] M. Ilton et al., "The principles of cascading power limits in small, fast biological and engineered systems," *Science*, vol. 360, no. 6387, 2018, Art. no. eaao1082.